VISCO-ACOUSTIC FINITE-DIFFERENCE MODELING IN THE FREQUENCY DOMAIN

B. ARNTSEN, A.G. NEBEL and L. AMUNDSEN

Statoil Research Centre, Postuttak, N-7005 Trondheim, Norway.

(Received June 21, 1997; revised version accepted November 7, 1997)

ABSTRACT

Arntsen, B., Nebel, A.G. and Amundsen, L., 1998. Visco-acoustic finite-difference modeling in the frequency domain. *Journal of Seismic Exploration*, 7: 45-64.

Frequency domain finite-difference modeling schemes have the advantage that synthetic data can be obtained for additional source positions at minimal extra computational cost. Attenuation of seismic waves can be easily included, and the method is well suited for implementation on a high performance parallel computer system. We show how to derive and implement an accurate finite-difference modeling scheme in the frequency domain. In contrast to earlier work, the scheme employs highly accurate approximations to the spatial derivatives, increasing accuracy and decreasing computational cost. Numerical solutions for simple models are given illustrating the straightforward inclusion of visco-acoustic attenuation.

KEY WORDS: visco-acoustic, attenuation, finite-difference, frequency domain, error analysis.

INTRODUCTION

Forward modeling of seismic waves has proven a useful tool in exploration and production seismology. Numerical solutions of the wave equation using finite-difference or fine-element methods are particularly useful as they provide complete synthetic seismograms including multiple reflections, surface waves and shear waves. Explicit finite-difference schemes formulated in the time domain have been the preferred methods used by the seismic industry the last 10-20 years. Examples of these schemes are found in Kelly et al. (1976), Holberg (1987), Virieux (1986), Levander (1988), Carcione (1992) and Robertson et al. (1994).

0963-0651/98/$5.00

Finite-difference schemes can also be implemented in the frequency domain leading to implicit methods which require the solution of large linear systems of equations. The important advantage is that direct solution methods are available that allow synthetic data to be obtained for additional source positions at minimal extra computational cost. Also attenuation of seismic waves can be easily and accurately modeled, and numerical dispersion due to time integration is removed. In the past, sufficient computer power has not been available to allow efficient solutions of large systems of linear equations. However, given the recent development of cost-effective parallel computer systems the necessary computational resources are now at hand. Frequency domain finite-difference methods are particularly well suited for parallel computer architectures since computations can proceed independently for each frequency.

Several workers have proposed and implemented frequency domain finite-difference or finite-element schemes. Among these are Drake (1972), Marfurt (1984), Pratt (1990) and Pratt and Worthington (1990). We extend the scheme proposed by Pratt and Worthington (1990) to include optimized approximations to the numerical derivatives leading to greatly improved accuracy for coarse grids. This allows the use of either larger models for the same cost, or reduced computational cost for the same size of models. We use the optimized differentiators proposed by Holberg (1987). The resulting implicit finite-difference scheme can be formulated as a system of linear equations. The matrix formulation of this system requires the inversion of a large sparse matrix, which reduces to a matrix similar to the one found by Pratt and Worthington (1990) in the case of a simple, unoptimized classical approximation to the derivative. Attenuation is included in the scheme by allowing the wave velocity to be complex. The numerical dispersion introduced by the frequency domain finite-difference scheme is analyzed by comparing the numerical solution in a homogeneous medium with an analytical plane-wave solution. We find that the simple classical approximation to derivatives requires at least 15-20 grid points per wavelength to be usable; in contrast, the optimized scheme is accurate down to 2.5 grid points per wavelength. It is also found that the accuracy of the optimized scheme starts to decrease above approximately 10 grid points per wavelength.

The next two sections cover the theory and error analysis of the 'classical' and optimized finite-difference schemes followed by a section with numerical examples.

IMPLICIT FINITE-DIFFERENCE SCHEME

We consider a visco-acoustic medium with bulk modulus κ and density ρ. The two-dimensional (2-D) equations of motion expressed in the frequency domain can be written

$$\omega^2\rho(x,z)u_x(x,z,\omega) = \partial_x p(x,z,\omega) \ ,$$

$$\omega^2\rho(x,z)u_z(x,z,\omega) = \partial_z p(x,z,\omega) \ ,$$

and

$$p(x,z,\omega) = -\kappa(x,z,\omega)[\partial_x u_x(x,z,\omega) + \partial_z u_z(x,z,\omega)] + s'(x,z,\omega) \ . \qquad (1)$$

Here ω is the frequency, u_x and u_z are the particle displacements in the x- and z-directions and p is the pressure. s' is the source of volume injection type. Note that the bulk modulus κ is in general complex and a function of frequency. Eliminating the particle displacements from the equations in (1), we get the acoustic wave equation (suppressing the frequency dependence in the arguments of p)

$$[\omega^2/\kappa(x,z)]p(x,z) + \partial_x[1/\rho(x,z)]\partial_x p(x,z) + \partial_z[1/\rho(x,z)]\partial_z p(x,z)$$

$$= s(x,z,\omega). \qquad (2)$$

Here $s(x,z,\omega) = [\omega^2/\kappa(x,z,\omega)]s'(x,z,\omega)$. The finite-difference method discretizes equation (2) on a regular grid and then solves the resulting equations with respect to the pressure p. We choose a grid with a grid interval equal to Δx in the x-direction and Δz in the z-direction such that

$$x = (i - 1)\Delta x, i = 1, 2, \ldots, N_x \ ,$$

and (3)

$$z = (j - 1)\Delta z, j = 1, 2, \ldots, N_z \ .$$

Here N_x is the number of grid points in the x-direction, while N_z is the number of grid points in the z-direction. The following shorthand will be used throughout

$$p(x,z) = p[(i - 1)\Delta x,(j - 1)\Delta z] = p(i,j) \ . \qquad (4)$$

The derivatives in equation (2) are approximated with centered differences since this is more accurate than forward or backward differences. The simplest possible centered difference approximation to a derivative is

$$\partial_x p(x,z)\big|_{x-\Delta x/2,z} \approx d_x^-[p(i,j)] = (1/\Delta x)[p(i,j) - p(i - 1,j)] \ , \qquad (5)$$

and

$$\partial_x p(x,z)\big|_{x+\Delta x/2,z} \approx d_x^+[p(i,j)] = (1/\Delta x)[p(i + 1,j) - p(i,j)] \ . \qquad (6)$$

The superscripts $-$ and $+$ indicate that the centered differences use one grid point behind or in front of the current grid point, respectively. This implies that the derivative is evaluated halfway between the current grid point and the grid point in front thereof, or halfway between the current grid point and the grid point behind it. For increased accuracy equations (5) and (6) can be

generalized to a higher-order approximation

$$d_x^- p(i,j) = (1/\Delta x) \sum_{k=1}^{l} \alpha_k [p(i + (k-1),j) - p(i-k),j)] \quad , \tag{7}$$

and

$$d_x^+ p(i,j) = (1/\Delta x) \sum_{k=1}^{l} \alpha_k [p(i + k,j) - p(i - (k-1),j)] \quad . \tag{8}$$

Equations (7) and (8) can be regarded as the convolution of the differentiator d_x^- or d_x^+ defined by the coefficients α_k, with the pressure p. The number of coefficients l is determined by the desired accuracy. The coefficients α_k are computed by an optimization procedure matching the Fourier spectrum of the differentiators with the spectrum of a perfect differentiator (Holberg, 1987).

Discretizing equation (2) and using equations (7) and (8) for differentiation in both the x- and z-directions, we get

$$[\omega^2/\rho(i,j)c^2(i,j)]p(i,j) + d_x^+ \rho^{-1}(i - (1/2),j) d_x^- p(i,j) + d_z^+ \rho^{-1}(i - (1/2),j) d_z^- p(i,j) = s(i,j) \quad , \tag{9}$$

where the notations $\rho(x-\Delta x/2,z) = \rho(i-1/2,j)$ and $\rho(x,z-\Delta z/2) = \rho(i,j-1/2)$ have been used. We have also introduced the wave velocity c using the relation $\kappa = \rho\, c^2$. The derivative of the pressure together with the density are now in effect defined on a separate ('staggered') grid displaced $\Delta x/2$ with respect to the regular grid defined in equation (4). The pressure p itself and the bulk modulus κ are defined on the main grid. Fig. 1 illustrates the use of staggered grids.

Equation (9) is a system of simultaneous linear equations relating the pressure p(i,j) at every grid point to the source s(i,j) and the acoustic parameters $\kappa(i,j)$ and $\rho(i,j)$. In order to solve these equations with respect to the pressure values, it is advantageous to recast equation (9) into matrix form. As a first step to achieving this, the discretely sampled functions are indexed according to a new index I given by

$$I = i + (j-1)N_x \quad , \quad i = 1,\ldots,N_x \quad , \quad j = 1,\ldots,N_z \quad . \tag{10}$$

Defining new quantities $G_I = p(i,j)$ and $S_I = s(i,j)$, using equation (10), the pressure p and the source s are recast as single-column vectors $\mathbf{G} = (G_1, G_2, \ldots, G_{N_x N_z})$ and $\mathbf{S} = (S_1, S_2, \ldots, S_{N_x N_z})$. Equation (9) can be written as a matrix equation

$$\mathbf{LG} = \mathbf{S} \ . \tag{11}$$

Here **L** is a square matrix of size $N_x N_z$ times $N_x N_z$. The structure of the matrix **L** is in general characterized by a diagonal band of width $4l - 1$ and $4l - 2$ 'fringe' sub-diagonals. l is here the number of coefficients used in the differentiators. Below is a sketch of the structure of **L** in the simple case of $l=1$, which correspond to the 'classical' finite-difference scheme. Bullets represent non-zero values.

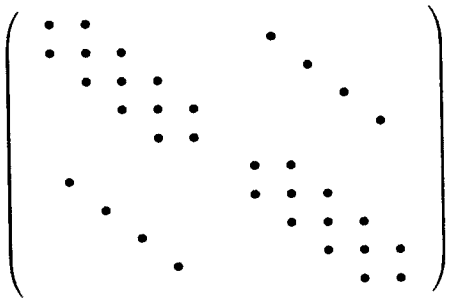

(12)

The wave velocity is in general assumed to be complex and frequency-dependent. This allows for a straightforward description of a visco-acoustic medium, as only the value of the complex velocity changes for different visco-acoustic models. This, in fact, only changes the main diagonal of **L**.

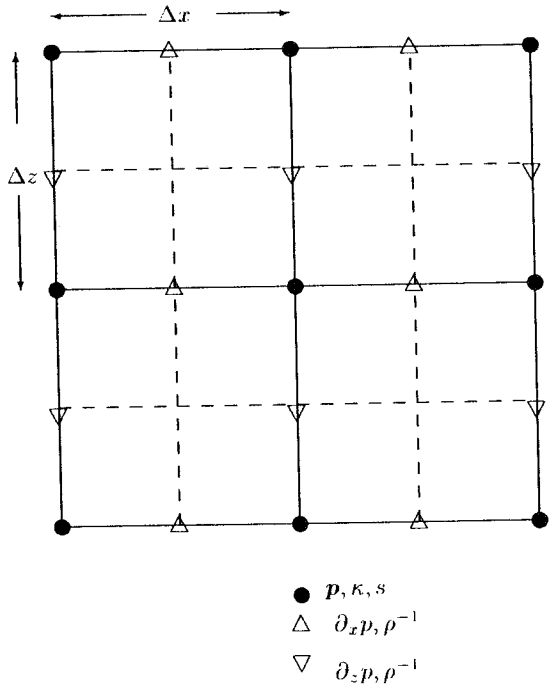

Fig. 1. Staggered grids used for implementing finite-difference scheme.

Boundary conditions at the edges of the computational grid are of course of great importance to the detailed form of the solution of equation (11). We have used the same approach as that described by Pratt (1990). He essentially uses a modified form of the absorbing boundary conditions introduced by Clayton and Enquist (1977).

Equation (11) can now, in principle, be solved using a standard numerical method for solving linear systems of equations. In general, these solution methods could be divided into two classes: direct and iterative methods. We have chosen to use a direct method, which is discussed in the section on numerical examples.

Causality of the solution cannot be directly enforced in the frequency domain, since we are, in fact, solving a time-harmonic problem. However, it is reasonable to assume that the Fourier transform of the corresponding time-domain problem with zero initial conditions is equal to the solution of equation (11). The time-domain solution is then recovered by an inverse Fourier transform.

ERROR ANALYSIS

The discrete form of the wave equation given by equation (9) is an approximation to the exact wave equation and its solution will consequently contain errors. The magnitudes of these errors depend on the discretization intervals Δx and Δz and can be interpreted in terms of frequency dependent phase and group velocities. In this section we investigate these errors by using an exact plane wave solution for a homogeneous medium

$$p(i,j) = \exp[ik_x(i-1)\Delta x + ik_z(j-1)\Delta z] \quad , \tag{13}$$

where $i = 1,..,N_x$ and $j = 1,...,Nz$. k_x and k_z are the wave numbers in the x- and z-directions, given by

$$k_x = k \sin(\theta)$$
and (14)
$$k_z = k \cos(\theta) \quad .$$

The wavenumber is $k = \omega/c_0$ and θ is the angle between the vertical direction and the direction of wave propagation. c_0 is the wave velocity.

Inserting equation (14) into equation (9) with the density constant equal to 1, and zero source term, one obtains

$$[\omega^2/c_0^2(i,j)]p(i,j) + d_x^+ d_x^- p(i,j) + d_z^+ d_z^- p(i,j) = 0 \quad . \tag{15}$$

Equation (15) leads to the expression

$$\omega/kc_0 = c/c_0 = \sqrt{[(\hat{k}_x/k)^2 + (\hat{k}_z/k)^2]} \quad , \tag{16}$$

where

$$\hat{k}_x/k = [M\sin(\theta)/2\pi]\sqrt{[-A_0 - 2\sum_{m=1}^{2l-1} A_m\cos\{2\pi m/M\sin(\theta)\}]} \quad , \tag{17}$$

and

$$\hat{k}_z/k = [M\cos(\theta)/2\pi]\sqrt{[-A_0 - 2\sum_{m=1}^{2l-1} A_m\cos\{2\pi m/M\cos(\theta)\}]} \quad . \tag{18}$$

The coefficients A_m, $m = 1, \ldots, 2l - 1$ are functions of the differentiator coefficients α_k, $k = 1, \ldots, l$. The number of grid points per wavelength, M, is related to the wave numbers k_x and k_z by

$$\begin{aligned} M &= 2\pi/(\sin(\theta)k_x\Delta x) \quad , \\ \text{and} \\ M &= 2\pi/(\cos(\theta)k_z\Delta z) \quad . \end{aligned} \tag{19}$$

Equation (16) is the dispersion relation for the plane wave given by equation (13) and relates frequency, wave velocity and wave numbers. Equations (17) and (18) relate the wave numbers to the grid discretization intervals Δx and Δz. If the discretization is perfect and no errors are introduced, then the right-hand side of equation (16) is identically equal to 1 for all wave numbers k_x and k_z. Any deviation from 1 is an error and is caused by the discretization of the wave equation.

Using equations (17) and (18) in equation (16) one gets an expression for the relative phase velocity c/c_0 as a function of propagation angle θ and number of wavelengths per grid points, M. In the simple case of $l = 1$, $A_0 = -2$ and equation (18) reduces to

$$\begin{aligned} \hat{k}_x/k &= (M/2\pi)\sqrt{[2 - 2\cos\{2\pi/M\sin(\theta)\}]} \quad , \\ \text{and} \\ \hat{k}_z/k &= (M/2\pi)\sqrt{[2 - 2\cos\{2\pi/M\cos(\theta)\}]} \quad . \end{aligned} \tag{20}$$

Figs. 2 and 3 show the relative phase velocity c/c_0 given by equations (16) and (20) plotted as a function of the number of grid points per wavelength M and the propagation angle θ. The differentiator used in this case corresponds to the 'classical' finite-difference operator. Figs. 4 and 5 show the relative phase velocity in which the number of coefficients α_k in the differentiators is 8.

Figs. 2 and 3 clearly show that the differentiator with length equal to 1 can only be used when the number of grid points per wavelength is larger than 15-20. Comparing the phase velocities for different angles of propagation it is clear that the error in phase velocity for the differentiator with length 1 is smallest when the plane wave propagates at an angle of 45 degrees to the vertical, although this difference is not very large. This is easily understood if one considers the fact that the number of grid points per *apparent* wavelength, M_x and M_z, in the x- and z-directions is given by

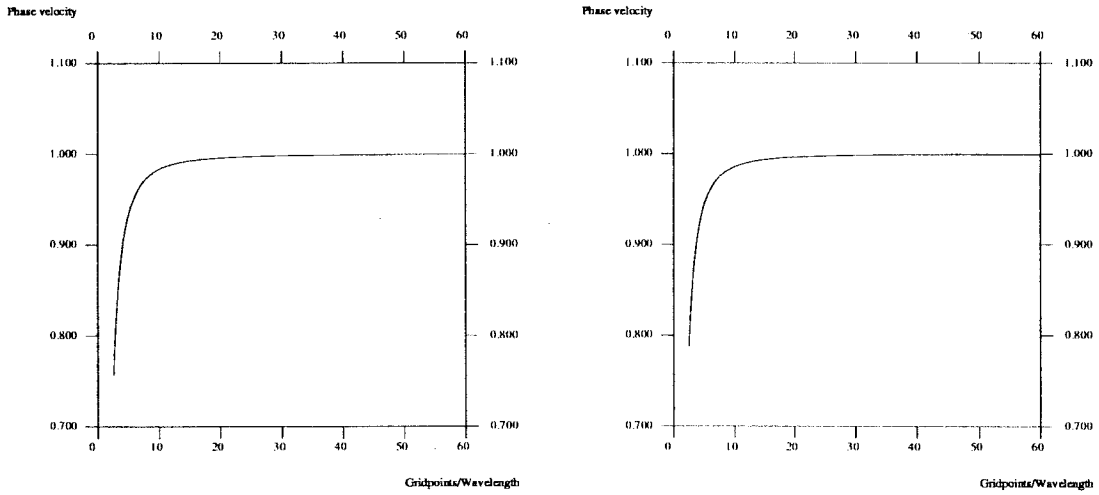

Fig. 2. Relative phase velocity using differentiators with length $l = 1$ and angle of propagation $\theta = 0$ (left) and $\theta = 15$ (right).

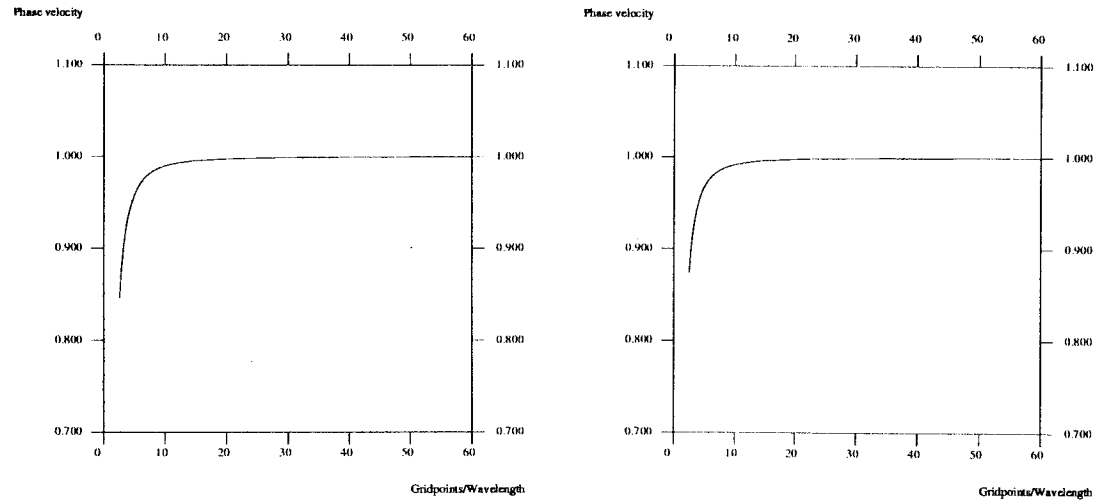

Fig. 3. Relative phase velocity using differentiators with length $l = 1$ and angle of propagation $\theta = 30$ (left) and $\theta = 45$ (right).

$$M_x = M/\sin(\theta) \quad , \tag{21}$$

and

$$M_z = M/\cos(\theta) \quad . \tag{22}$$

For the same frequency, the number of grid points per apparent wavelength (M_x and M_z) in the x- or z- direction is always larger than (or equal to) the number of grid points (M) in the direction of propagation. Now, our finite-difference scheme is designed using differentiators [equation (7)] which are designed independently along the x- or z-axis. These differentiators perform best for large values of the number of grid points per apparent wavelength.

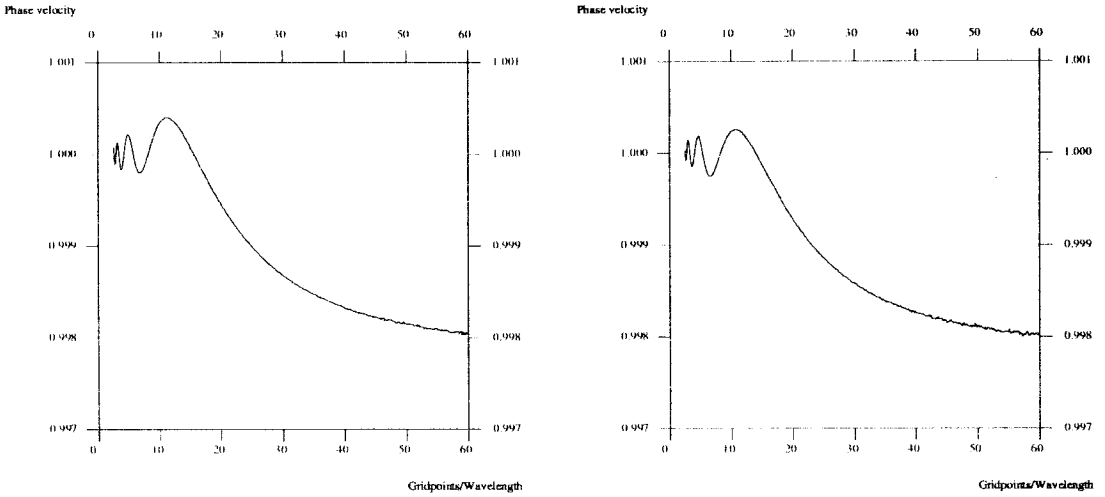

Fig. 4. Relative phase velocity using differentiators with length $l = 8$ and angle of propagation $\theta = 0$ (left) and $\theta = 15$ (right).

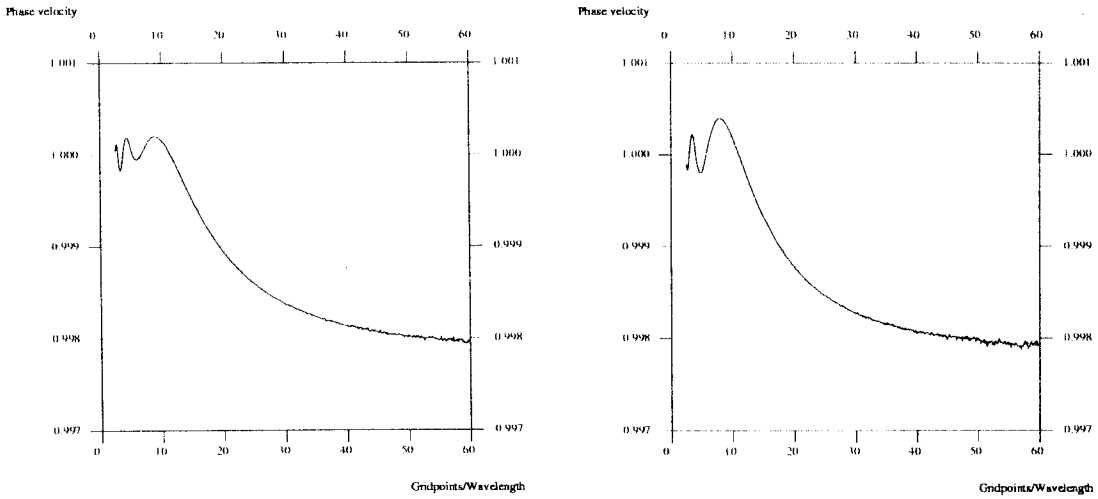

Fig. 5. Relative phase velocity using differentiators with length $l = 8$ and angle of propagation $\theta = 30$ (left) and $\theta = 45$ (right).

Hence, errors will be smaller if the direction of propagation is not coincident with one of the coordinate axes. Figs. 4 and 5 correspond to Figs. 2 and 3, except that the number of coefficients now used is equal to 8. Note the change of scale on the vertical axis in Figs. 4 and 5 relative to Figs. 2 and 3. The error in phase velocity is dramatically reduced, and is less than 0.003 for all values of the number of grid points per wavelength of practical interest. The error is an oscillating function for values of M less than approximately 10 grid points per wavelength, but increases almost monotonically for values of M larger than 10. The error in phase velocity changes somewhat as the angle of incidence changes, but this is due to the same mechanism as explained above for the differentiator with length equal to 1.

The group velocity measures the speed of energy transport and is defined by

$$c_g/c_0 = (\partial\omega/\partial k)/c_0 \quad . \tag{23}$$

For a homogeneous medium $c_g/c_0 = 1.0$.

Using equation (16) in equation (23) leads to

$$c_g/c_0 = [(1/\Delta x)\sin(\theta)B + (1/\Delta z)\cos(\theta)C]/\sqrt{[(\hat{k}_x/k)^2 + (\hat{k}_z/k)^2]} \quad , \tag{24}$$

where

$$B = \sum_{m=1}^{m=2l-1} mA_m \sin[mM/\sin(\theta)] \quad ,$$

and (25)

$$C = \sum_{m=1}^{m=2l-1} mA_m \sin[mM/\cos(\theta)] \quad ,$$

Equation (24) is the relative group velocity as a function of propagation angle θ and the number of grid points per wavelength. The group velocity measures the speed of physical energy transport, and is a better measure of the quality of a finite-difference scheme than the phase velocity.

Figs. 6 and 7 show the relative group velocity in the case of a simple differentiator with length equal to 1, while Figs. 8 and 9 show the relative group velocity in the case of optimized differentiators with length equal to 8. Note the change of scale on the vertical axis of Figs. 8 and 9 relative to Figs. 6 and 7. From the figures it is seen that the error in group velocity is somewhat larger than the error in phase velocity, but behaves in general as the error in phase velocity. The differentiator with length equal to 1 can not be used with any degree of confidence below approximately 15-20 grid points per wavelength,

while the long differentiator with length equal to 8 can be used for all values of grid points per wavelength of practical interest.

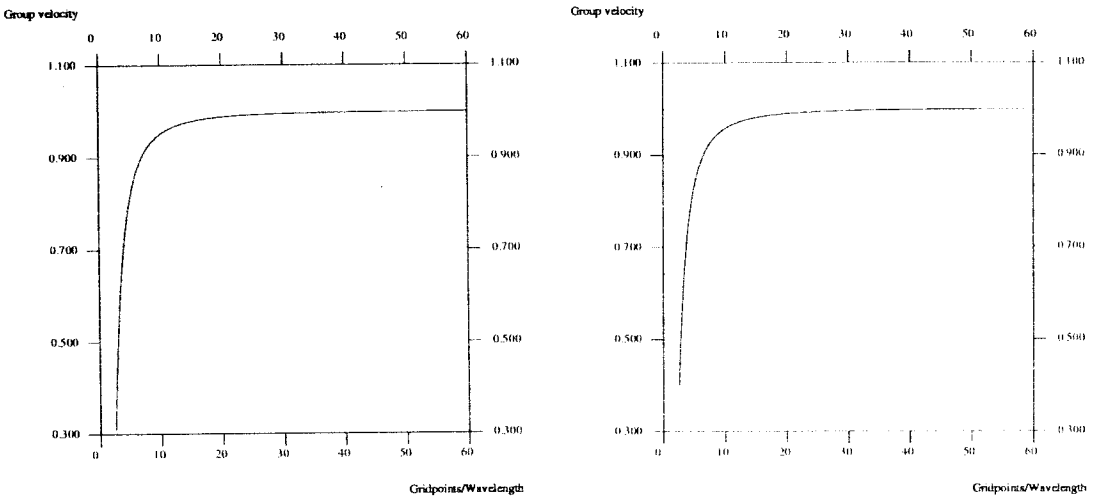

Fig. 6. Relative group velocity using differentiators with length $l = 1$ and angle of propagation $\theta = 0$ (left) and $\theta = 15$ (right).

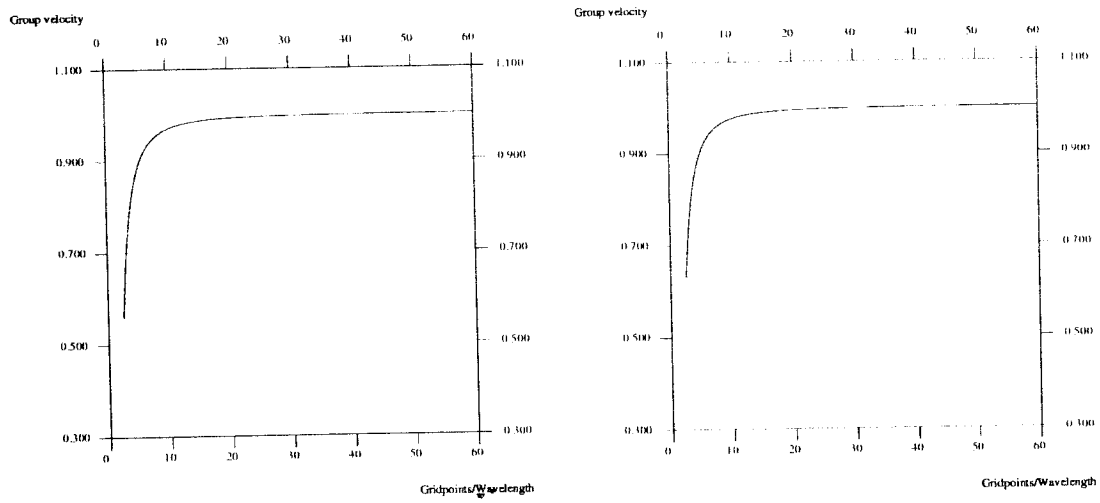

Fig. 7. Relative group velocity using differentiators with length $l = 1$ and angle of propagation $\theta = 30$ (left) and $\theta = 45$ (right).

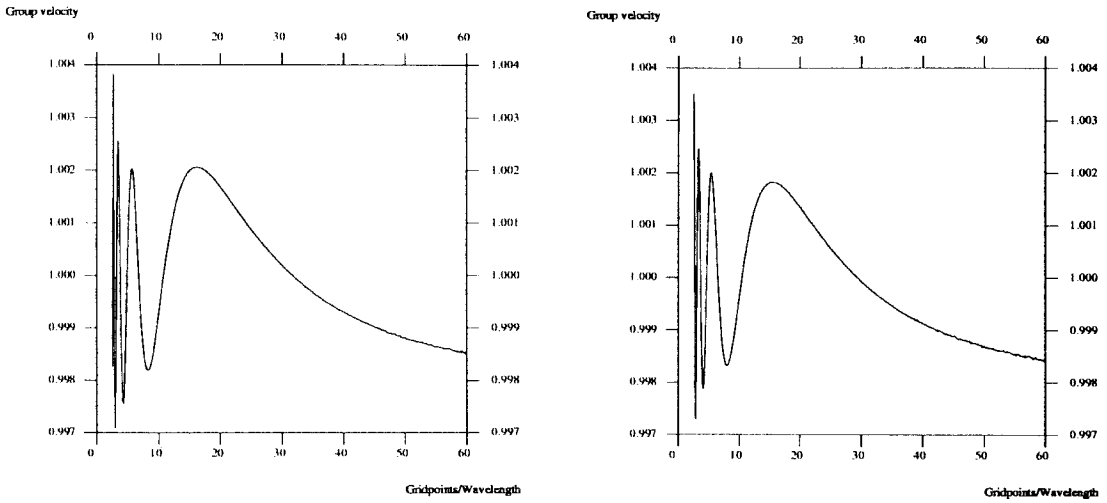

Fig. 8. Relative group velocity using differentiators with length $l = 8$ and angle of propagation $\theta = 0$ (left) and $\theta = 15$ (right).

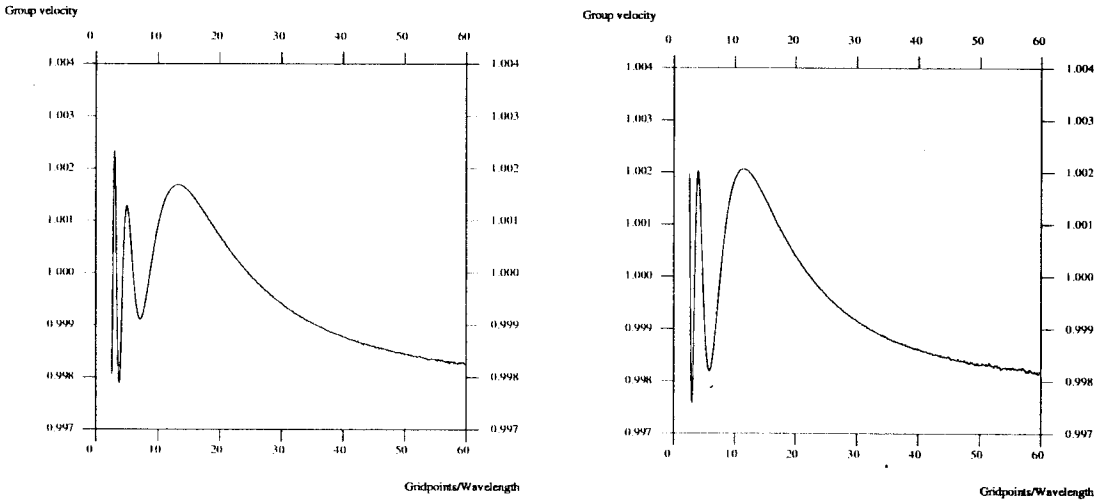

Fig. 9. Relative group velocity using differentiators with length $l = 8$ and angle of propagation $\theta = 30$ (left) and $\theta = 45$ (right).

NUMERICAL EXAMPLES

In this section simple numerical examples showing solutions of equation (11) for simple acoustic and visco-acoustic models are shown.

First a homogeneous model is considered. A source with Gaussian time dependence was positioned in the center of the model, which had a lateral extent of 400 m in the horizontal and vertical directions. A grid interval equal to 4 m was used, implying that the number of grid points in each direction was 200. The wave velocity was chosen equal to 2000 m/s and the maximum frequency

was 62.5 Hz. Equation (11) was solved for 33 different frequencies, and the pressure as a function of time was obtained by Fourier transformation. To avoid numerical problems with aliasing along the time axis, we used the concept of complex frequency (Mallick and Frazer, 1987). The numerical solution of the linear system of equations given by (11) was obtained using a standard off-the-shelf equation solver designed for sparse systems using an LU decomposition technique. No attempt was made to exploit the inherent simple structure of the matrix **L**. Fig. 10 shows the computed pressure in the homogeneous model at six different instants of time. As a check on the numerical solution, Fig. 11 shows the analytical solution plotted at the same time instants.

Fig. 12 shows the numerical solution for a visco-acoustic medium corresponding to a standard linear solid. (Ben-Menahem and Singh, 1981). The phase velocity is in this case complex and given by

$$c^2 = [c_0^2 + (\omega/\omega_r)^2 c_\infty^2 + i\omega/\omega_r(c_\infty^2 - c_0^2)]/[1 + (\omega/\omega_r)^2] \quad . \tag{26}$$

Here $c_0 = 2000$ m/s and $c_\infty = 2500$ m/s are the phase velocities in the limit of zero and infinite frequencies, respectively. ω_r is a reference frequency and is equal to 250 s^{-1}. Fig. 12 shows that the wave propagating in the visco-acoustic medium is clearly attenuated and dispersed compared with the purely acoustic wave shown in Fig. 11.

Fig. 13 shows the pressure at six different instants of time using the inhomogeneous visco-acoustic model shown in Fig. 14. The grid intervals in the x- and z-directions were equal to 4 m, while the maximum frequency was 62.5Hz. The number of frequencies was equal to 33. The density was kept constant. In Fig. 15 the pressure is displayed as a function of time at six different depths. Figs. 13 and 15 show quite clearly how the pressure wave field is reflected and distorted by the inhomogeneous model.

CONCLUSIONS

A frequency domain finite-difference scheme for acoustic wave propagation has been given. The scheme uses optimized differentiators and is more effective than a classical scheme using unoptimized differentiators. The scheme is implicit and requires the solution of a large system of linear equations. The error analysis reveals that the classical scheme requires at least 15-20 grid points per wavelength to achieve an accuracy comparable with the scheme using optimized differentiators. The optimized scheme is most accurate when the number of grid points is less than approximately 10. Above this point the accuracy decreases in a systematic way as the number of grid points per wavelength is increased.

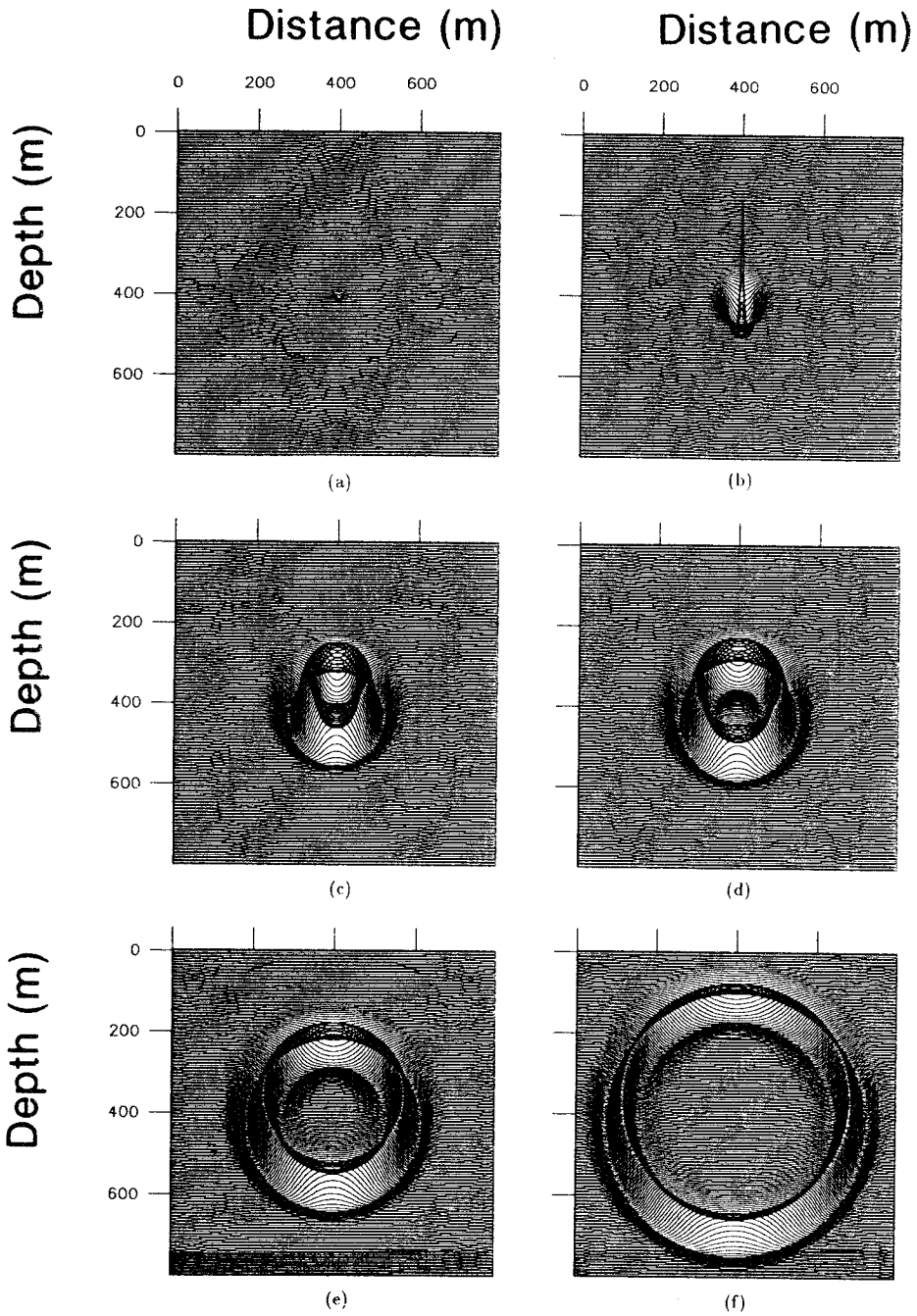

Fig. 10. Numerical solution of the pressure for the homogeneous model without attenuation at times (a) 16 ms, (b) 48 ms, (c) 96 ms, (d) 112 ms, (e) 144 ms, and (f) 200 ms.

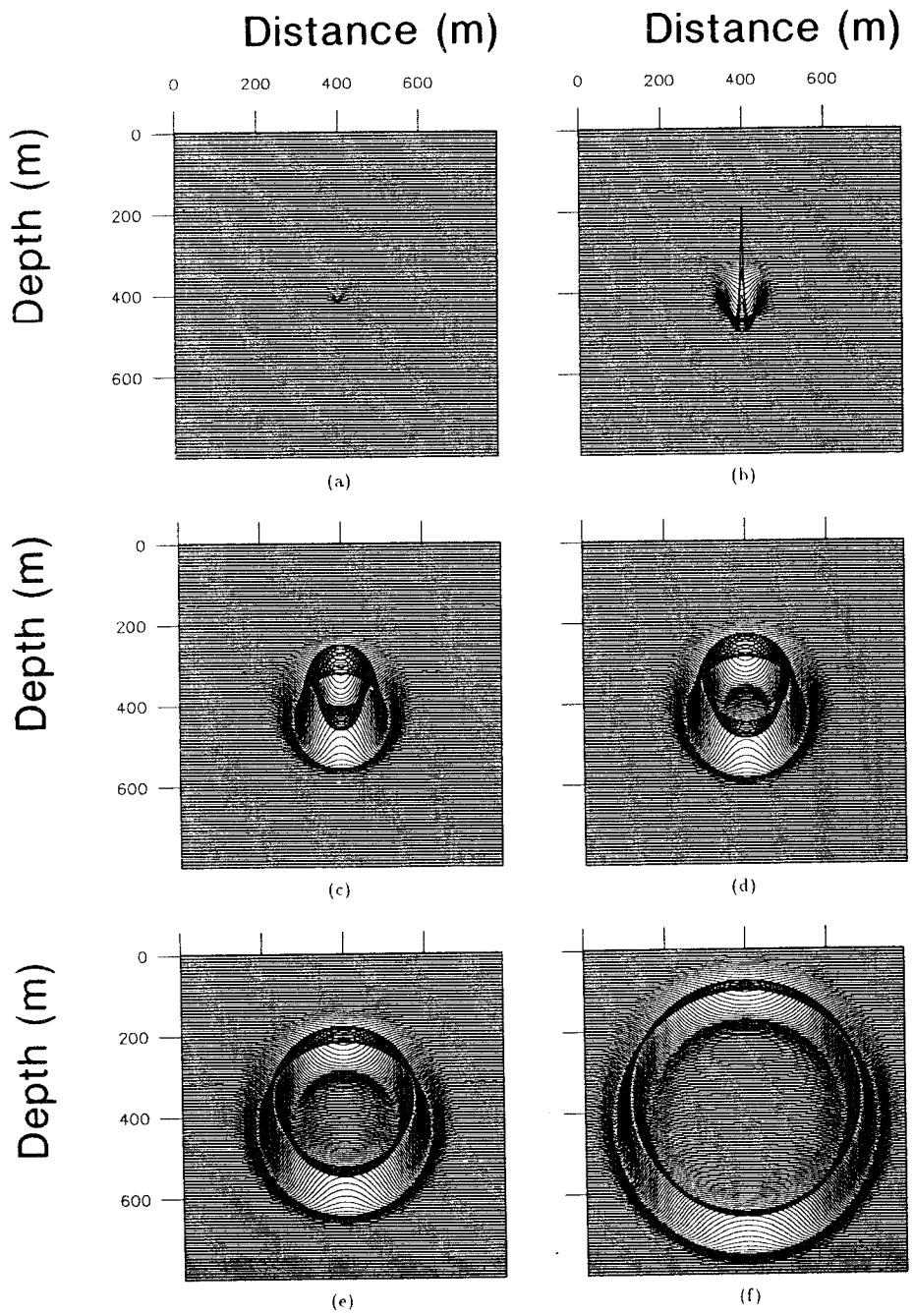

Fig. 11. Analytical solution of the pressure for the homogeneous model without attenuation at times (a) 16 ms, (b) 48 ms, (c) 96 ms, (d) 112 ms, (e) 144 ms, and (f) 200 ms.

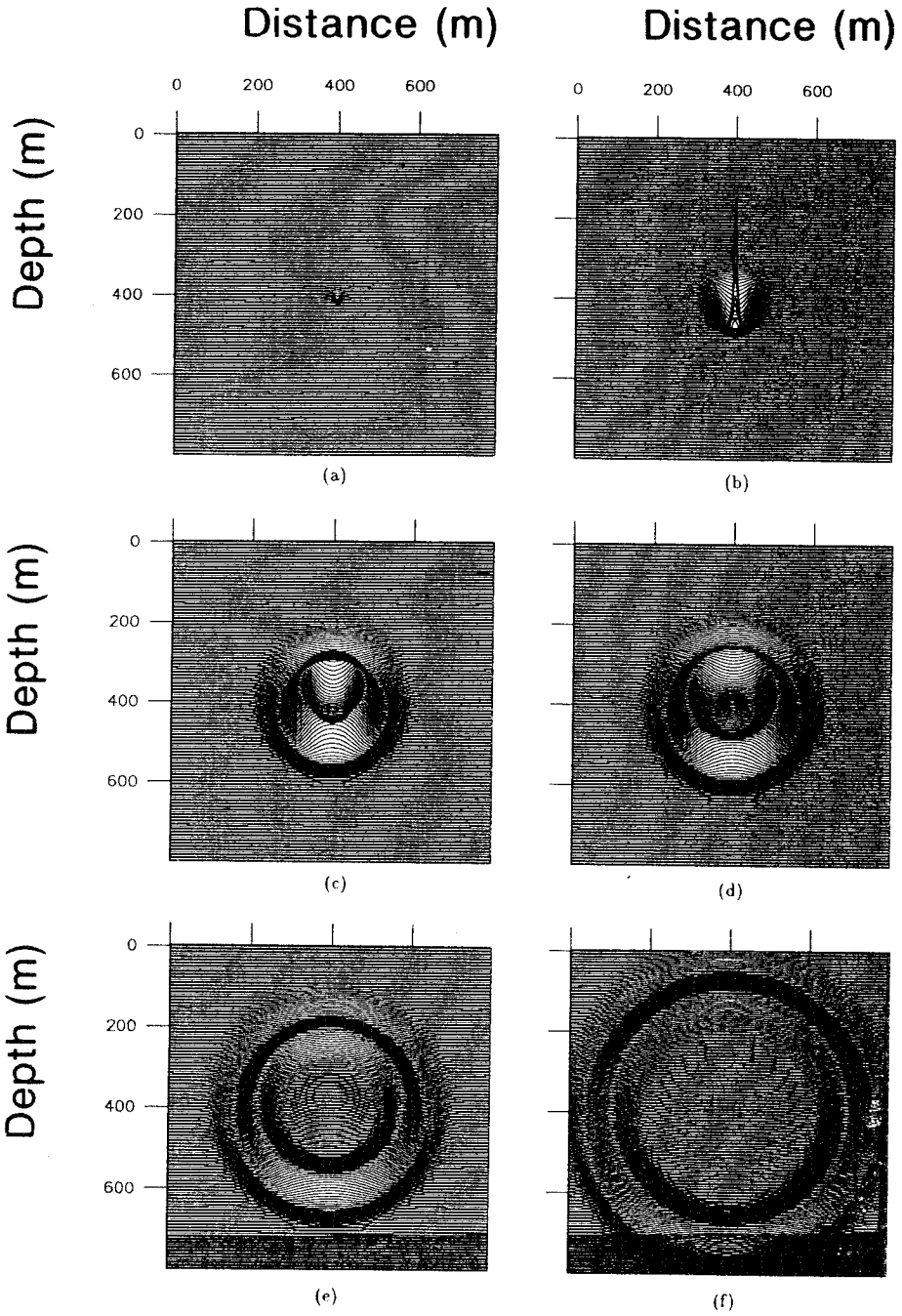

Fig. 12. Numerical solution of the pressure for the homogeneous model including attenuation at times (a) 16 ms, (b) 48 ms, (c) 96 ms, (d) 112 ms, (e) 144 ms, and (f) 200 ms.

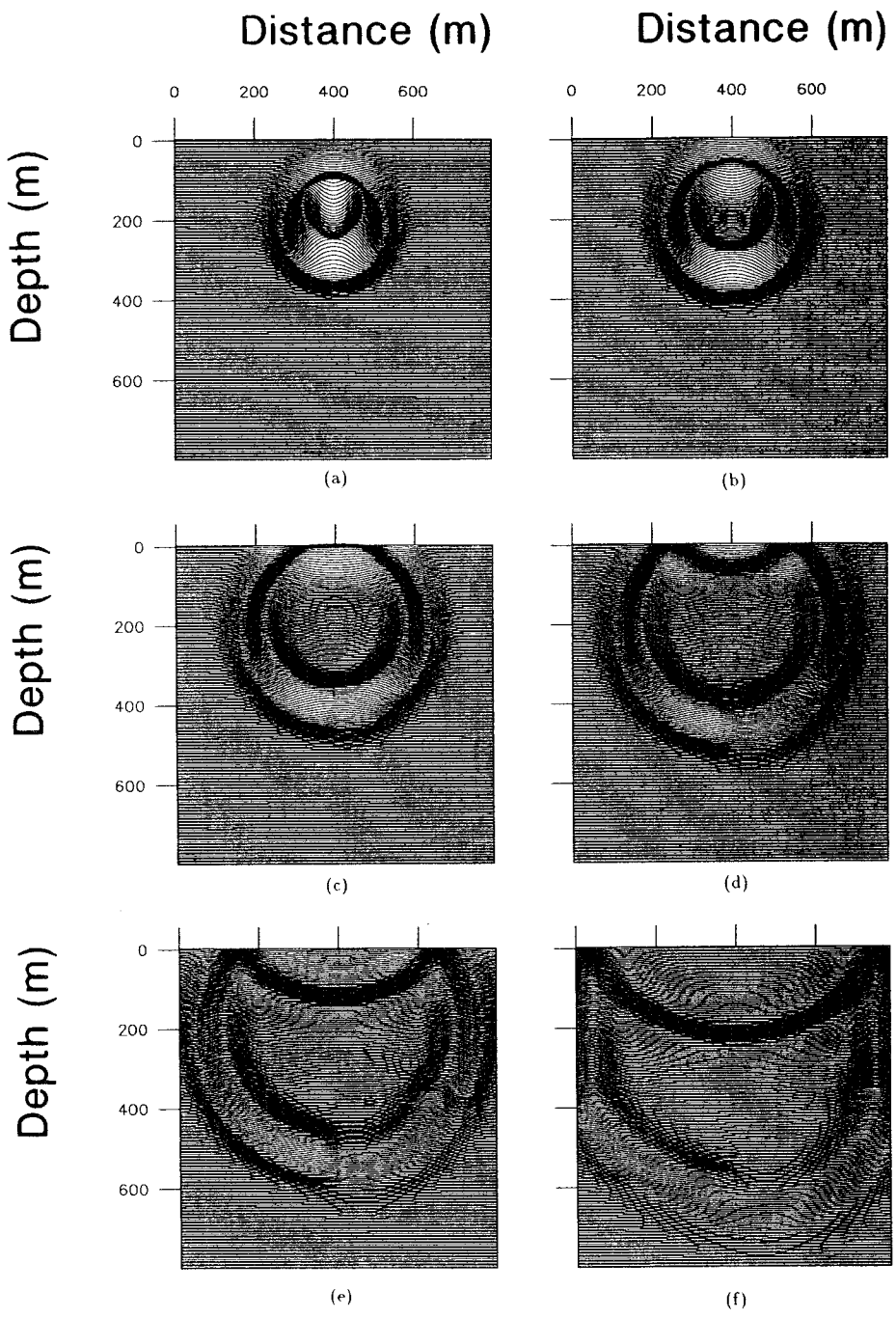

Fig. 13. Numerical solution of the pressure for the inhomogeneous visco-acoustic model at times (a) 96 ms, (b) 112 ms, (c) 144 ms, (d) 168 ms, (e) 200 ms, and (f) 248 ms.

The linear equations were solved using a standard LU decomposition technique designed for sparse systems. This method has the significant advantage that obtaining the solutions for additional source positions (i.e., different right-hand side vectors) is computationally inexpensive once the LU decomposition of the **L**-matrix has been performed.

Numerical examples showed that solutions of the linear systems of equations can be obtained in a straightforward way, even for models of reasonable size. Also, introduction of absorption via complex wave velocity is straightforward and easy to accomplish.

A new linear system must be solved for each frequency, but since these are almost computationally independent, solutions of these systems could occur in parallel. The parallel architecture of many new computer systems is very well suited for this type of task, making efficient frequency domain finite-difference modeling possible.

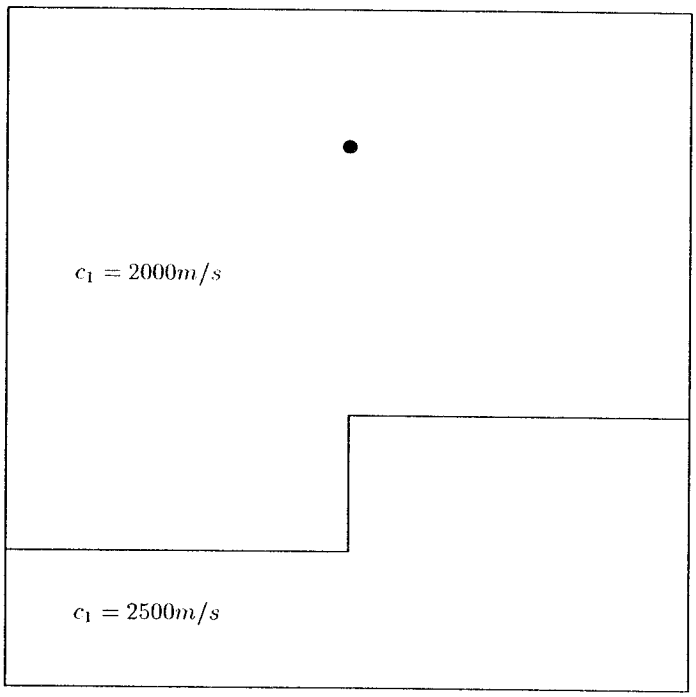

Fig. 14. Inhomogeneous visco-acoustic model.

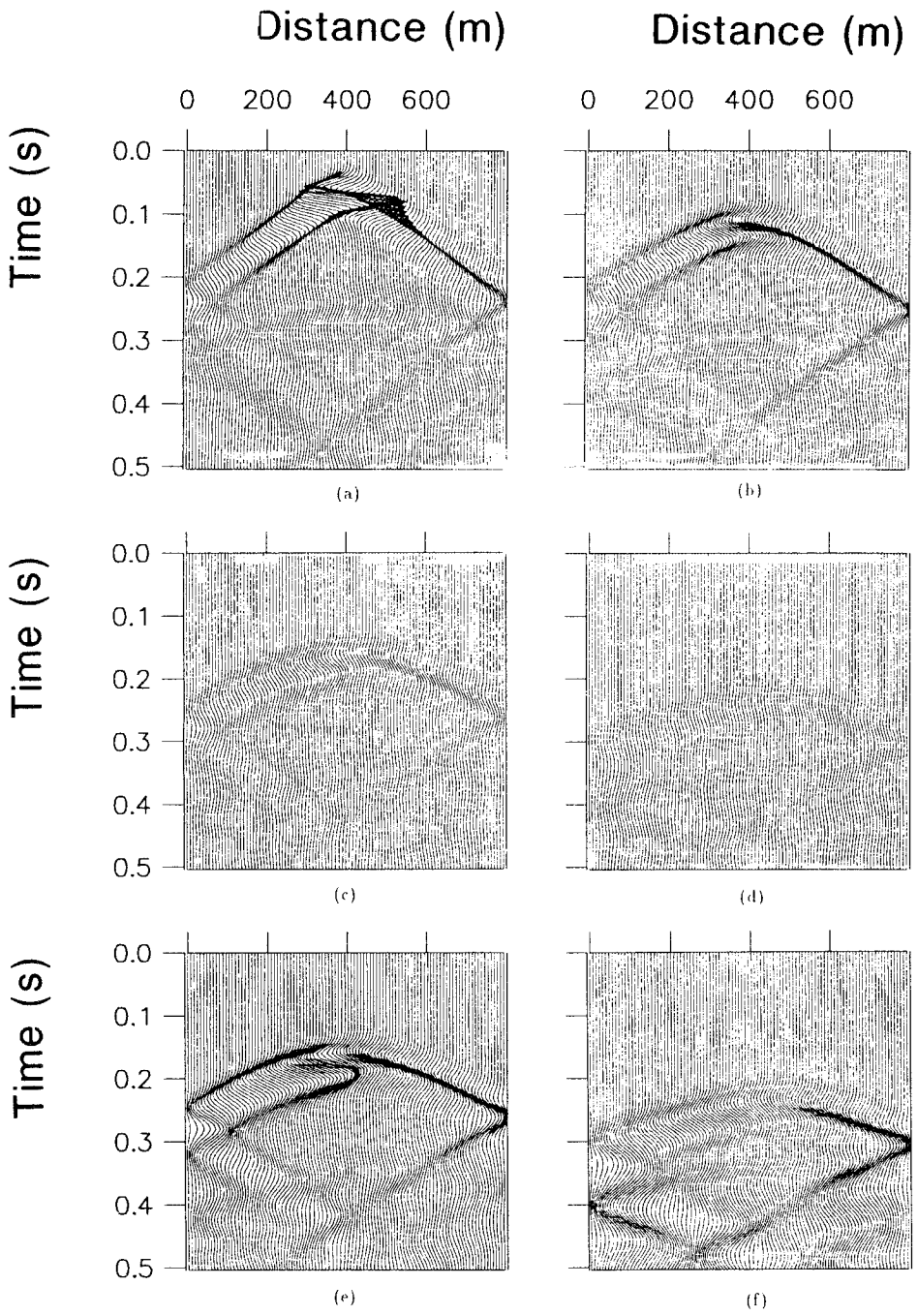

Fig. 15. Numerical solution of the pressure for the inhomogeneous visco-acoustic model at depths (a) 240 m, (b) 360 m, (c) 480 m, and (d) 680 m. (e) and (f) show the numerical solution at depths 480 m and 680 m where the amplitudes have been scaled by a factor of 10.

REFERENCES

Ben-Menahem, A. and Singh, S.J., 1981. Seismic waves and sources. Springer-Verlag, Berlin.

Carcione, J.M., Kosloff, D., Behle, A. and Seriani, G., 1992. A spectral scheme for wave propagation simulation in 3-D elastic-anisotropic media. Geophysics, 57: 1593-1607.

Clayton, R.W. and Enquist, B., 1981. Absorbing boundary conditions for acoustic and elastic wave equations. Bull. Seismol. Soc. Am., 67: 1529-1540.

Drake, L.A., 1977. Love and Rayleigh waves in nonhorizontally layered media. Bull. Seismol. Soc. Am., 62: 1241-1258.

Holberg, O., 1987. Computational aspects of the choice of operator and sampling interval for numerical differentiation in large-scale simulation of wave phenomena. Geophys. Prosp., 37: 629-655.

Kelly, K.R., Ward, R.W., Treitel, S. and Alford, R.M., 1976. Synthetic seismograms: a finite-difference approach. Geophys. Prosp., 41: 2-27.

Levander, A.R., 1988. Fourth-order finite-difference P-SV seismograms. Geophysics, 53: 1425-1436.

Mallick, S. and Frazer, L.N., 1987. Practical aspects of reflectivity modeling. Geophysics, 52: 1355-1364.

Marfurt, K.J., 1984. Accuracy of finite-difference and finite-element modeling of the scalar and elastic wave equations. Geophysics, 49: 533-549.

Pratt, R., 1990. Frequency-domain elastic wave modeling by finite differences. Geophysics, 55: 626-632.

Pratt, R. and Worthington, M.H., 1990. Inverse theory applied to multi-source cross-hole tomography. Part 1: Acoustic wave-equation method. Geophys. Prosp., 38: 287-310.

Pratt, R. and Worthington, M.H., 1990. Inverse theory applied to multi-source cross-hole tomography. Part 2: Elastic wave-equation method. Geophys. Prosp., 38: 311-329.

Robertson, J.O.A., Blanch, J.O. and Symes, W.W., 1994. Viscoelastic finite-difference modeling. Geophysics, 59: 1444-1456.

Virieux, J., 1986. P-SV wave propagation in heterogeneous media: Velocity-stress finite-difference method. Geophysics, 51: 889-901.